Fundamentals of negative refractive index optical trapping: forces and radiation pressures exerted by focused Gaussian beams using the generalized Lorenz-Mie theory

Leonardo A. Ambrosio* and Hugo E. Hernández-Figueroa

School of Electrical and Computer Engineering (FEEC), Department of Microwaves and Optics (DMO), University of Campinas (Unicamp), 13083-970 Campinas–SP, Brazil
**leo@dmo.fee.unicamp.br*

Abstract: Based on the generalized Lorenz-Mie theory (GLMT), this paper reveals, for the first time in the literature, the principal characteristics of the optical forces and radiation pressure cross-sections exerted on homogeneous, linear, isotropic and spherical hypothetical negative refractive index (NRI) particles under the influence of focused Gaussian beams in the Mie regime. Starting with ray optics considerations, the analysis is then extended through calculating the Mie coefficients and the beam-shape coefficients for incident focused Gaussian beams. Results reveal new and interesting trapping properties which are not observed for commonly positive refractive index particles and, in this way, new potential applications in biomedical optics can be devised.

OCIS codes: (350.4855) Optical tweezers or optical manipulation; (160.3918) Metamaterials; (350.3618) Left-handed materials; (080.0080) Geometric optics; (290.4020) Mie theory.

References and links

1. A. Ashkin and J. M. Dziedzic, "Optical trapping and manipulation of viruses and bacteria," Science **235**(4795), 1517–1520 (1987).
2. M. W. Berns, W. H. Wright, B. J. Tromberg, G. A. Profeta, J. J. Andrews, and R. J. Walter, "Use of a laser-induced optical force trap to study chromosome movement on the mitotic spindle," in *Proceedings of the National Academy of Science of the United States of America* **86**, (1989), pp. 7914–7918.
3. S. B. Smith, Y. Cui, and C. Bustamante, "Overstretching B-DNA: the elastic response of individual double-stranded and single-stranded DNA molecules," Science **271**(5250), 795–799 (1996).
4. G. D. Wright, J. Arlt, W. C. K. Poon, and N. D. Read, "Experimentally manipulating fungi with optical tweezers," Mycoscience **48**, 15–19 (2007).
5. A. Ashkin, "Optical trapping and manipulation of neutral particles using lasers," in *Proceedings of the National Academy of Science of the United States of America* **94**, (1997), pp. 4853–4860.
6. K. C. Neuman and S. M. Block, "Optical trapping," Rev. Sci. Instrum. **75**(9), 2787–2809 (2004).
7. D. P. O'Neal, L. R. Hirsch, N. J. Halas, J. D. Payne, and J. L. West, "Photo-thermal tumor ablation in mice using near infrared-absorbing nanoparticles," Cancer Lett. **209**(2), 171–176 (2004).
8. L. A. Ambrosio and H. E. Hernández-Figueroa, "Inversion of gradient forces for high refractive index particles in optical trapping," Opt. Express **18**(6), 5802–5808 (2010).
9. V. G. Veselago, "The Electrodynamics of Substances with Simultaneously Negative Values of ε and μ," Sov. Phys. Usp. **4**, 509–514 (1968).
10. D. R. Smith, W. J. Padilla, D. C. Vier, S. C. Nemat-Nasser, and S. Schultz, "Composite medium with simultaneously negative permeability and permittivity," Phys. Rev. Lett. **84**(18), 4184–4187 (2000).
11. R. A. Shelby, D. R. Smith, and S. Schultz, "Experimental verification of a negative index of refraction," Science **292**(5514), 77–79 (2001).
12. N. Engheta and R. Ziolkowski, "A positive future for double-negative metamaterials," IEEE Trans. Microw. Theory Tech. **53**(4), 1535–1556 (2005).
13. N. Engheta and R. Ziolkowski, *Metamaterials – Physics and Engineering Explorations* (IEEE press, Wiley-Interscience, John Wiley & Sons, 2006).
14. C. Caloz and T. Itoh, *Electromagnetic Metamaterials: Transmission Line Theory and Microwave Applications* (IEEE press, Wiley-Interscience, John Wiley & Sons, 2006).

#133019 - $15.00 USD Received 6 Aug 2010; revised 13 Oct 2010; accepted 17 Oct 2010; published 4 Nov 2010

15. L. A. Ambrosio and H. E. Hernández-Figueroa, "Trapping double negative particles in the ray optics regime using optical tweezers with focused beams," Opt. Express **17**(24), 21918–21924 (2009).
16. A. Ashkin, "Forces of a single-beam gradient laser trap on a dielectric sphere in the ray optics regime," Biophys. J. **61**(2), 569–582 (1992).
17. A. B. Stilgoe, T. A. Nieminen, G. Knöener, N. R. Heckenberg, and H. Rubinsztein-Dunlop, "The effect of Mie resonances on trapping in optical tweezers," Opt. Express **16**(19), 15039–15051 (2008).
18. Y. Hu, T. A. Nieminen, N. R. Heckenberg, and H. Rubinsztein-Dunlop, "Antireflection coating for improved optical trapping," J. Appl. Phys. **103**, 093119 (2008).
19. G. Mie, "Beiträge zur Optik Trüber Medien, Speziell Kolloidaler Metallösungen," Ann. Phys. **25**, 377–445 (1908).
20. G. Gouesbet and G. Gréhan, "Sur la généralisation de la théorie de Lorenz-Mie," J. Opt. (Paris) **13**, 97–103 (1982).
21. B. Maheu, G. Gouesbet, and G. Gréhan, "A concise presentation of the generalized Lorenz-Mie theory for arbitrary incident profile," J. Opt. (Paris) **19**, 59–67 (1988).
22. G. Gouesbet, G. Gréhan and B. Maheu, "Expressions to compute the coefficients g_n^m in the generalized Lorenz-Mie theory using finite series," J. Opt. (Paris) **19**, 35–48 (1988).
23. C. F. Bohren and D. R. Huffmann, *Absorption and Scattering of Light by Small Particles* (Wiley-Interscience, John Wiley & Sons, 1983).
24. G. Gouesbet, G. Gréhan, and B. Maheu, "Localized interpretation to compute all the coefficients g_n^m in the generalized Lorenz-Mie theory," J. Opt. Soc. Am. A **7**, 998–1007 (1990).
25. K. F. Ren, G. Gouesbet, and G. Gréhan, "Integral localized approximation in generalized lorenz-mie theory," Appl. Opt. **37**(19), 4218–4225 (1998).
26. G. Gouesbet and J. A. Lock, "Rigorous justification of the localized approximation to the beam-shape coefficients in generalized Lorenz-Mie theory. I. On-axis beams," J. Opt. Soc. Am. A **11**, 2503–2515 (1994).
27. G. Gouesbet and J. A. Lock, "Rigorous justification of the localized approximation to the beam-shape coefficients in generalized Lorenz-Mie theory. II. Off-axis beams," J. Opt. Soc. Am. A **11**, 2516–2525 (1994).
28. H. Polaert, G. Gréhan, and G. Gouesbet, "Forces and torques exerted on a multilayered spherical particle by a focused Gaussian beam," Opt. Commun. **155**, 169–179 (1998).
29. K. F. Ren, G. Gréhan, and G. Gouesbet, "Radiation pressure forces exerted on a particle arbitrarily located in a Gaussian beam by using the generalized Lorenz-Mie theory, and associated resonance effects," Opt. Commun. **108**, 343–354 (1994).
30. K. F. Ren, G. Gréhan, and G. Gouesbet, "Symmetry relations in generalized Lorenz-Mie theory," J. Opt. Soc. Am. A **11**, 1812–1817 (1994).
31. A. Ashkin and J. M. Dziedzic, "Optical levitation by radiation pressure," Appl. Phys. Lett. **19**, 283–285 (1971).
32. A. Ashkin and J. M. Dziedzic, "Stability of optical levitation by radiation pressure," Appl. Phys. Lett. **24**, 586–588 (1974).
33. A. Ashkin and J. M. Dziedzic, "Optical levitation in high vacuum," Appl. Phys. Lett. **28**, 333–335 (1976).
34. A. Ashkin and J. M. Dziedzic, "Feedback stabilization of optically levitated particles," Appl. Phys. Lett. **30**, 202–204 (1977).
35. A. Ashkin and J. M. Dziedzic, "Observation of light scattering from nonspherical particles using optical levitation," Appl. Opt. **19**(5), 660–668 (1980).
36. K. R. Fen, *Diffusion des Faisceaux Feuille Laser par une Particule Sphérique et Applications aux Ecoulements Diphasiques* (Ph.D thesis, Faculté des Sciences de L'Université de Rouen, 1995).
37. J. B. Pendry, "Negative refraction makes a perfect lens," Phys. Rev. Lett. **85**(18), 3966–3969 (2000).

1. Introduction

Optical micromanipulation of molecules and biological organelles has revolutionized biomedical research and opened the way for an enormous quantity of promising studies evolving viruses and bacteria [1], chromosomes [2], DNA [3], fungi [4], human cells, general particles [5,6] and, maybe the most interesting, new proposals in cancer treatment [7].

Technological developments in the area of optical trapping are evident during the past forty years since the first experiments on Bell labs, by A. Ashkin. In a series of experiments, he put the theory behind tridimensional optical micromanipulation on solid grounds. Initially based on a pair of counter propagating moderately diverging Gaussian beams (2-beam traps) to capture randomly diffused small particles, he further improved the experimental setup to achieve levitation schemes (levitation traps), where the scattering forces exerted on a particle by one single vertical beam were used to cancel the effects of gravity. Finally, the adoption of one single focused beam paved the way for the systems now known as optical tweezers by allowing particles to be easily stretched and manipulated. A robust theory in damage-free optical traps of particles by using infrared laser beams is now available.

#133019 - $15.00 USD Received 6 Aug 2010; revised 13 Oct 2010; accepted 17 Oct 2010; published 4 Nov 2010

Optical traps are based on momentum transfer from the photons of the laser beam to the trapped particle, thus giving rise to axial and transverse forces that, in certain conditions, can pull them to high intensity regions of the beam. The relation between the repulsion/attraction profile and the relative refractive index n_{rel} between the particle (refractive index n_p) and the surrounding medium (n_m) in which it is immersed leads to a well known behavior: particles with $n_{rel} > 1$ will always be directed towards high intensity regions of the incident beam, whereas for $n_{rel} < 1$ the contrary can be observed: the particle will be directed away from these regions. For high refractive index particles (e.g., $n_{rel} > 3$ or 4), however, this relation is no longer valid due to the prevailing of repulsive axial (scattering) forces [8].

Because of the increasing interest in metamaterial applications, especially among those with negative refractive index (NRI), it is plausible to ask ourselves what would happen to a NRI particle in an optical tweezers system. Would it be trapped in the same way as a positive refractive index (PRI) particle?

This special type of material is not a recent development. In fact, its properties are known since the final 60's, when russian physicist Veselago predicted the hypothetical existence of NRI materials and consistently established a theoretical background for subsequent works [9]. It took, however, more than thirty years for scientific community to realize the importance and the revolution behind Veselago's medium, when the first experimental evidence of negative permittivity and permeability was published [10,11].

Since then, research in metamaterial phenomena rapidly flourished (for a review of the subject see, e.g [12]. For further theoretical and experimental background, see [13,14]). Interesting applications were proposed such as perfect lenses and optical cloaking. Transmission-line analogies can predict most of one- and two-dimensional behaviors of NRI materials. Although one- and two-dimensional resonant and non-resonant structures were developed and experimentally verified, 3D NRI structures are still a challenge. The search for a homogeneous, isotropic, linear dielectric NRI material remains, and we can possibly benefit from their properties in the near future.

In a previous work, we presented some basic principles behind what can be called "negative refractive index" or "double-negative" optical trapping, without, however, going into a profound analysis. Using ray optics considerations, gradient and scattering optical forces exerted on hypothetical spherical NRI particles were analyzed and it was concluded that new displacement behaviors could be observed [15] and that the limit $n_{rel} = 1$ (in the NRI analogue, $n_{rel} = -1$) does not play such a significant role as it does for PRI particles.

This paper is the natural extension of [15] and is organized as follows: section 2 reviews and significantly expands the analysis of [15] for negative refractive index optical trapping using geometrical optics considerations, the main results concerning optical forces being then outlined; section 3 introduces the Mie coefficients and the equivalence between Snell's law inversion and the differences in the Mie scattering coefficients when n_{rel} goes from $n_{rel} > 0$ to $n_{rel} < 0$. A brief resume of the well-known generalized Lorenz-Mie theory (GLMT) is also presented. Finally, section 4 is devoted to discussing the application of the GLMT – and focused Gaussian beams – to NRI optical trapping. Transverse and longitudinal radiation pressure cross-sections (radiation pressure forces) are then numerically evaluated. In the final section, our conclusions are presented.

2. Ray optics

Suppose an arbitrary laser beam with wavelength λ, propagating along a medium of refractive index n_m, impinges on an arbitrary NRI dielectric spherical particle with radius a. The particle is assumed to be homogeneous, isotropic and linear, with a refractive index n_p. In this section we consider that the ray optics condition, i.e., $a >> \lambda$, is tacitly satisfied, so that we may visualize the impinging beam as being composed of a set of infinite rays, all of them contributing to the total force exerted on the particle.

#133019 - $15.00 USD Received 6 Aug 2010; revised 13 Oct 2010; accepted 17 Oct 2010; published 4 Nov 2010

It is well-known that when a ray hits a positive refractive index particle with an incident angle θ_i, part of its incident power is reflected with the same incident angle and part of it is transmitted according to Snell's law, i.e., $\sin\theta_i = n_{rel}\sin\theta_t$, where θ_t is the transmission angle and $n_{rel} = n_p/n_m$. Subsequent reflections/refractions give rise to a multiple reflection/transmission diagram.

Due to the momentum transfer from the ray to the particle, one can analytically calculate the individual axial and transverse forces (F_z, z-directed, F_y, y-directed, according to the convention adopted in Fig. 1(c) of [15]) by summing up the contribution of all rays leaving the particle, i.e., these individual forces are given by the contribution of the rays with power PR, PT^2, PT^2R, PT^2R^2, …, PT^2R^m,…, P being the power of the original incident ray, R and T the Fresnel coefficients of reflection and transmission, respectively, their expressions depending upon the polarization of the incident beam, and m an integer number [16].

For a NRI particle, however, due to the inversion of Snell's law, the first transmitted ray into this particle is deflected with a "negative" angle θ_t, so that the individual transverse and axial forces must change accordingly (for instance, replace α by $2\theta_i + 2\theta_t$ and β by $\pi + 2\theta_t$ in Appendix I of [16]. This leads to Eqs. (1) and (2) of [15]).

Let us suppose that $n_{rel} = -1$, so that $R = 0$ ($T = 1$) for a circularly polarized beam. Furthermore, assume that one of its infinite rays is a z-propagating ray impinging the NRI particle with an incident angle $\theta_i = 45°$. For this particular ray, the first associated transmitted ray (with the same power as the incident ray, $PT = P$) is now y-directed, and the final ray exiting the particle propagates along $-z$, in a situation that resembles total reflection ($R = 1$, $T = 0$), except by the fact that the counter propagating final ray is spatially y-shifted from the incident ray. But conservation of linear momentum results in the same repulsive (away from the laser beam source) axial force. Of course, this situation would never happen for a PRI particle. Even though the axis of the incident ray does not coincide with the z-axis, being only parallel to it, there is no net transverse force. For rays with $\theta_i > 45°$, $F_y > 0$ (i.e., repulsive), whereas $F_y < 0$ (attractive) for rays with $\theta_i < 45°$. We can generalize this result by stating that, given a negative relative refractive index n_{rel}, there is always an specific incident angle $\theta_{i,s}$ to which the following are true: $F_y = 0$ for $\theta_i = \theta_{i,s}$; $F_y > 0$ for $\theta_i > \theta_{i,s}$; and $F_y < 0$ for $\theta_i < \theta_{i,s}$. Axial forces are always repulsive for any single ray.

Figures 1(a) and 1(b) reveals the intensity of the axial force F_y for a PRI spherical particle as a function of both θ_i and n_p for a circularly polarized incident ray, where $n_m = 1.33$ is assumed. According to the coordinate system adopted [15], $F_y > 0$ ($F_y < 0$) corresponds to a repulsive (attractive) axial force. Two zero force lines, $F_y = 0$, have been highlighted in Fig. 1(b). The first one, $F_y(n_{rel} = 1)$, is the matched case where $R = 0$, $T = 1$, and $\theta_i = \theta_t$. The second zero-force line, F_y ($n_{rel} = n_c$), can be interpreted as the limit situation where, given an incident ray with an incident angle θ_i, an increase of the relative refractive index n_{rel} (above a critical value n_c) implies on the prevailing of the first reflected ray with power PR over all secondary rays of powers PT^2, PT^2R and so on [10]. The scattering (axial) force F_z is always positive, i.e., repulsive, as expected [16].

#133019 - $15.00 USD Received 6 Aug 2010; revised 13 Oct 2010; accepted 17 Oct 2010; published 4 Nov 2010

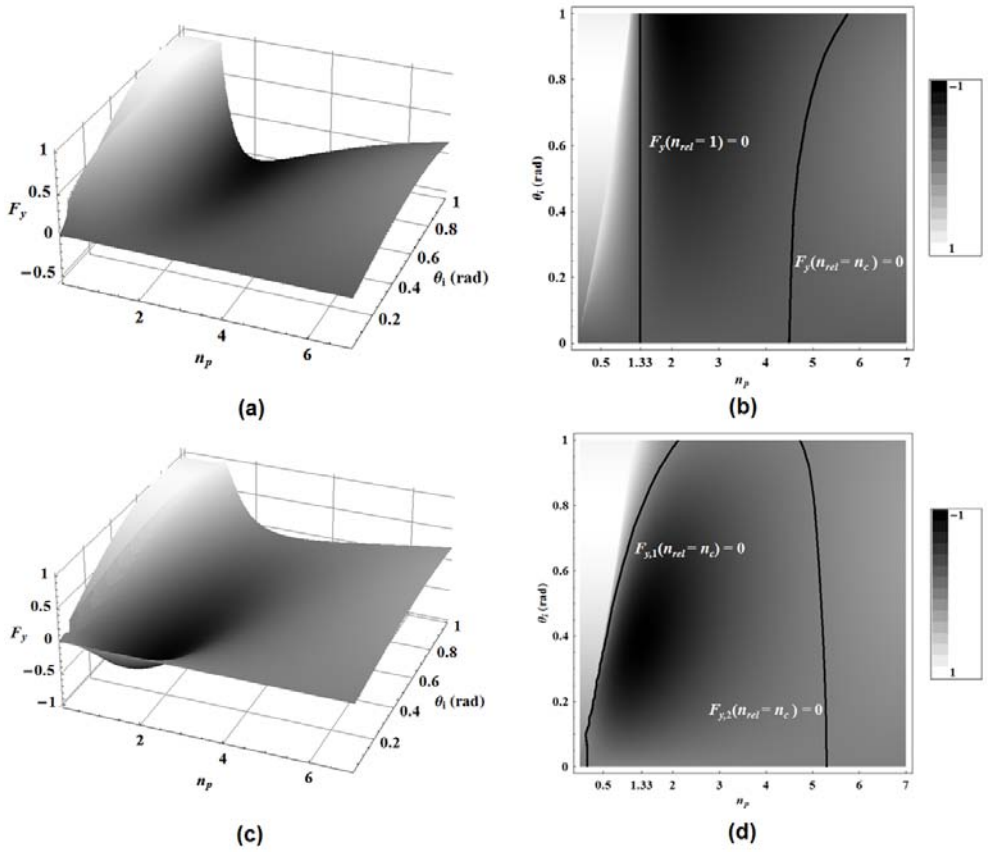

Fig. 1. Normalized (over $n_m P/c$) individual transverse force F_y as a function of both θ_i and n_p for a circularly polarized ray over (a) a PRI and (c) a NRI particle. The difference observed between these two cases leads to new trapping phenomena for $n_{rel} < 0$. (b) and (d) are the contour plots of (a) and (c), respectively.

Figures 1(c) and 1(d) are plots of F_y as function of n_p and θ_i. Two zero force lines, representing the $(n_{rel},\theta_i = \theta_{i,s})$ points where $F_y = 0$, are now highlighted in Fig. 1(d). Contrary to Fig. 1(b), transverse forces do not become zero when $|n_{rel}| = 1$. Note, furthermore, that in specifying n_{rel} we are actually imposing the constraint between the force and the incidence angle and, as shown in Fig. 2 for $n_{rel} = \pm 1.2$ and ± 0.8 (assuming the same values for the incident beam as before), the magnitude of the individual axial force exerted on a NRI particle can be significantly different from the PRI analogue.

A real situation can be used to illustrate how disparate these conclusions can be for both PRI and NRI optical trapping. Assume that the objective lens that focuses the Gaussian beam exiting the source has an associated numerical aperture $\theta_{NA} = 66°$, and that $0.5 < n_{rel} < 3$. In this way, for all incident rays that compose the focused Gaussian beam, if the centre of the particle is located close to the focal point, $\theta_i < \theta_{NA} = 66°$ and, according to Figs. 1(a) and 1(b), one can expect that an attractive (repulsive) transverse force will always occur whenever $1 < n_{rel} < 3$ $(0 < n_{rel} < 1)$.

But for $n_{rel} < 0$ the situation is a little bit more involved, as now each ray can produce an attractive or a repulsive transverse force depending upon its incidence angle, so that, theoretically, the trapping properties for NRI particles depends upon the shape of the incident laser beam. For example, we could, in principle, design a particular laser beam such that, for an specific n_{rel}, the particle will always be directed towards its high intensity regions, and

#133019 - $15.00 USD Received 6 Aug 2010; revised 13 Oct 2010; accepted 17 Oct 2010; published 4 Nov 2010

another laser beam such that, for the same n_{rel}, will always pull the particle towards nulls of intensity. This possibility is just impracticable for $n_{rel} > 0$.

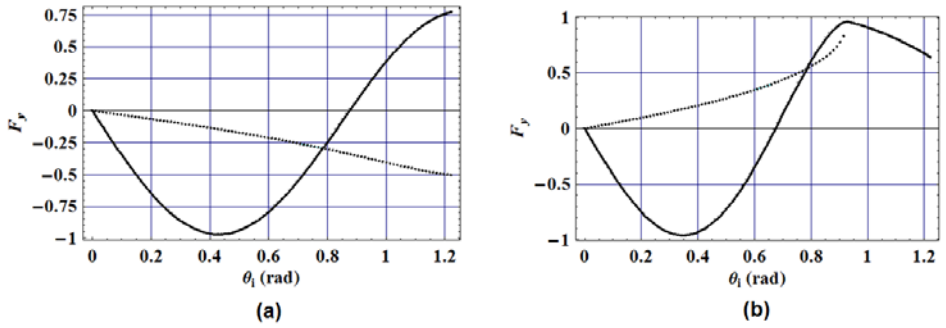

Fig. 2. Normalized (over $n_m P/c$) individual transverse force F_y as a function of θ_i for (a) n_{rel} = 1.2 (dotted) and –1.2 (solid) and (b) n_{rel} = 0.8 (dotted) and –0.8 (solid). Force profiles can significantly vary for NRI and PRI particles possessing the same (in modulus) electromagnetic parameters. In (b), total reflection occurs for $\theta_i > 0.9273$ rad.

When considering a global coordinate system, each ray of our focused Gaussian beam impinges on the particle with a different angle relative to the optical axis [15,16]. Thus, we must consider total axial and transverse forces relative to a tridimensional global coordinate system. Although the details concerning the calculation of total axial and transverse forces are outside the scope of this paper, the reader is referred to [15,16] for further details.

The total transverse force exerted on a PRI particle is plotted in Fig. 3(a) as function of both n_{rel} and the distance r between the centre of the particle and the optical axis of a circularly polarized focused Gaussian beam (θ_{NA} = 66°) with a beam waist w_0 = 1 μm. The particle is assumed to be on a plane transverse to the optical axis and containing the focal point of the beam (the beam waist centre). The radius of the particle is $a = 10\lambda$, λ = 1064 nm. One can see attractive (negative) forces for all n_{rel} just above 1 and repulsive (positive) forces for $0 < n_{rel} < 1$. Obviously, $\mathbf{F}_{transverse} = 0$ for $n_{rel} = 0$, as expected. It is interesting to note the inversion of this transverse force from attractive to repulsive for high refractive index particles. In terms of ray optics, this is due to the fact that, as n_{rel} increases, the power PR of the first reflected ray also increases, thus with a prevailing of repulsive forces [8]. As for the ripples, this is due to the vector nature of the optical force and, at least in the Mie regime, this phenomenon is associated with interference and resonance effects [17,18]. Figure 3(b) is a contour plot of Fig. 3(a).

Figure 4 is the equivalent of Fig. 3 for a NRI particle with the same parameters as before. In this situation, the transverse total force profile can be interpreted as follows: regardless of $n_{rel} \gtrsim 1$ or $n_{rel} \lesssim 1$, if the centre of the particle is close to the focus (beam waist centre), then it will always be attracted to the optical axis because transverse forces are attractive for low r. As $|n_{rel}|$ increases from zero, the range of possible r that still leads to attractive forces also increases but, above a certain distance, this force becomes repulsive, making optical trapping difficult to be achieved. There are no specific (constant) n_{rel} that makes $F_{transverse} = 0$, as in the PRI case (for $n_{rel} = 1$). Finally, one can compare the amplitudes of $F_{transverse}$ in both figures. Attractive $F_{transverse}$ forces can be much stronger than these same forces acting on the equivalent PRI particle. For $n = -1.31$, $F_{transverse}|_{\max} = -7.24$ (a.u.), whereas for $n = 1.31$, $F_{transverse}|_{\max} = -2.96$ (a.u.), more than two times the expected force for a conventional PRI particle. Resonance effects are also observed for NRI particles with high refractive indices.

#133019 - $15.00 USD Received 6 Aug 2010; revised 13 Oct 2010; accepted 17 Oct 2010; published 4 Nov 2010

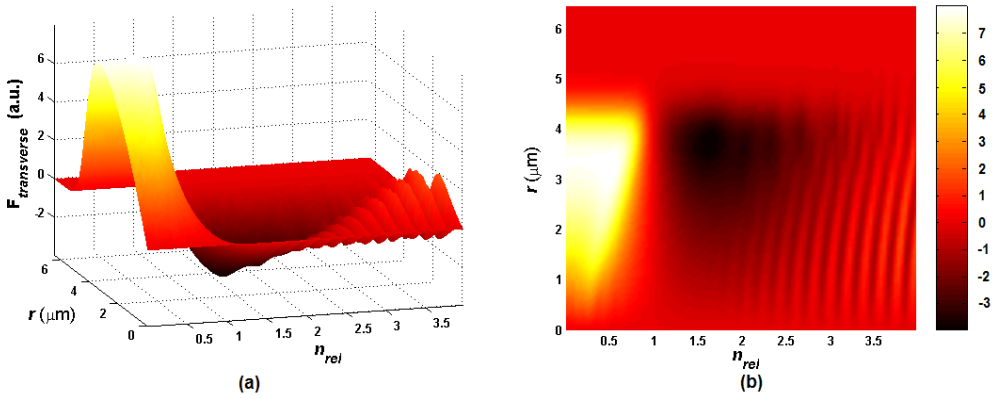

Fig. 3. (a) $F_{transverse}$ as a function of both n_{rel} and r for a PRI particle under the influence of a focused Gaussian beam with w_0 = 1000 nm. The particle has a radius $a = 10\lambda$, where λ = 1064 nm is the wavelength of the beam. When n_{rel} = 1, $F_{transverse}$ is always zero, as expected. (b) The contour plot of (a). Arbitrary units are adopted.

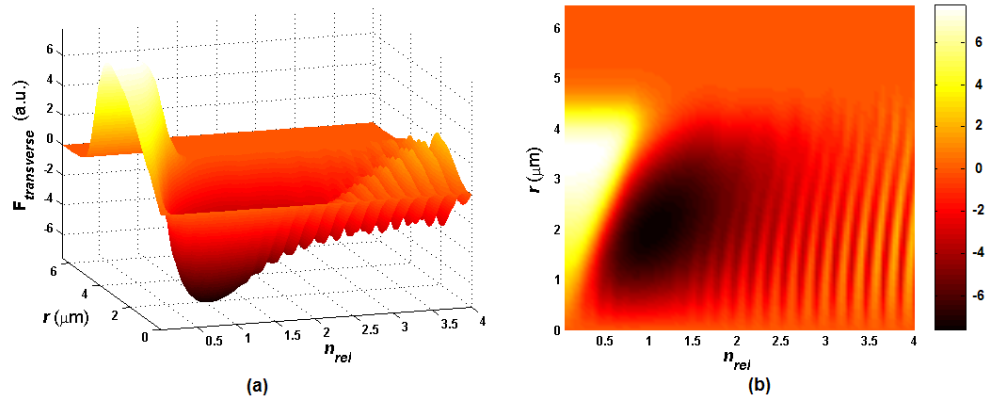

Fig. 4. (a) $F_{transverse}$ as a function of both n_{rel} and r for a NRI particle under the influence of the same laser beam and electromagnetic parameters as in Fig. 3. (b) The contour plot of (a). The same arbitrary units of Fig. 3 are adopted.

Although the results for geometrical optics are very interesting, we now go beyond ray optics and present a generalized theory capable of furnishing a deep physical meaning for the differences observed for the optical forces in NRI and PRI optical trapping. This is accomplished in the next sections by adopting the generalized Lorenz-Mie theory (GLMT).

3. Review of the generalized Lorenz-Mie theory and its extension to negative refractive indices

The GLMT is an extension of the Lorenz-Mie theory [19] for an incident beam of arbitrary shape and consists in expanding the incident electromagnetic field into a series of vector spherical harmonics, the coefficients of which being calculated by imposing the boundary conditions at the surface of the sphere and by making use of similar expressions for the scattered and internal fields [20–22].

In the framework of the Lorenz-Mie theory, in which the incident beam is a plane wave, the Mie scattering coefficients are known to be given as [23]

#133019 - $15.00 USD Received 6 Aug 2010; revised 13 Oct 2010; accepted 17 Oct 2010; published 4 Nov 2010

$$a_n = \frac{\mu n_{rel}\psi_n(n_{rel}x)\psi_n'(x) - \mu_p\psi_n(x)\psi_n'(n_{rel}x)}{\mu n_{rel}\psi_n(n_{rel}x)\xi_n'(x) - \mu_p\xi_n(x)\psi_n'(n_{rel}x)} \quad (1)$$

$$b_n = \frac{\mu_p\psi_n(n_{rel}x)\psi_n'(x) - \mu n_{rel}\psi_n(x)\psi_n'(n_{rel}x)}{\mu_p\psi_n(n_{rel}x)\xi_n'(x) - \mu n_{rel}\xi_n(x)\psi_n'(n_{rel}x)} \quad (2)$$

where μ_p and μ are the permittivity of the particle and its surrounding medium, respectively, ψ_n and ξ_n are Riccati-Bessel functions, n (not to be confused with n_{rel}, the relative refractive index) is an integer that ranges from 1 to + ∞ and $x = ka$ is the size parameter of the particle, k being the wave number of the incident wave. The primes indicate derivatives with respect to the argument of the Riccati-Bessel functions. These relations should remain the same regardless of the scatter being a NRI or a PRI particle, because the tangential components of the fields at the interface (surface of the particle) are not affected by the negative refractive index of the particle [9].

When an arbitrary beam is considered, the coefficients in the GLMT expansion are weighted, according to the shape of the beam, by the well-known beam-shape coefficients (BSC's) of the GLMT which, by adopting the integral localized approximation, can be written as [24,25]

$$g_{n,TE}^m = \frac{Z_n^m}{2\pi H_0}\int_0^{2\pi}\hat{G}\left[H_r(r,\theta,\phi)\right]e^{-im\phi}d\phi \quad (3)$$

$$g_{n,TM}^m = \frac{Z_n^m}{2\pi E_0}\int_0^{2\pi}\hat{G}\left[E_r(r,\theta,\phi)\right]e^{-im\phi}d\phi \quad (4)$$

which depends only on the radial component of the electric and magnetic fields E_r and H_r, a localization operator $\hat{G}$ and normalization factors Z_n^m, $-n < m < n$. Note that, in Eqs. (3) and (4), spherical coordinates (r,θ,ϕ) are assumed and, therefore, the incident beam must be changed to a spherical coordinate system accordingly (in this paper, we tacitly assume that the reader is familiarized with both the mathematical background and the notation adopted herein. As the BSC's are not altered whether the particle is of NRI or PRI nature, we shall not go into further details (for additional information see, e.g., [20–22,24,25] and references therein). All simulations and results presented in this paper assume a first-order Davis approximation for a focused Gaussian beam, as adopted by previous works [26,27], so that $g_{n,TE}^m$ and $g_{n,TM}^m$ in Eqs. (3) and (4) read, for a + z-propagating linearly x-polarized beam, as [26,27]:

$$g_{n,TE}^m = \frac{k_n^m}{2i}F^{Davis}(n+1/2,\pi/2)\sum_{j=0}^{\infty}\sum_{p=0}^{j}\Psi_{j,p}^{Davis}(n+1/2,\pi/2)\left(\delta_{j-2p+1,m}-\delta_{j-2p-1,m}\right) \quad (5)$$

$$g_{n,TM}^m = \frac{k_n^m}{2}F^{Davis}(n+1/2,\pi/2)\sum_{j=0}^{\infty}\sum_{p=0}^{j}\Psi_{j,p}^{Davis}(n+1/2,\pi/2)\left(\delta_{j-2p+1,m}+\delta_{j-2p-1,m}\right), \quad (6)$$

where k_n^m are normalization factors, $\Psi_{j,p}^{Davis}$ and F^{Davis} are functions of the spatial coordinates (x_0,y_0,z_0) of the beam (relative distance between the beam waist centre and the centre of the spherical particle) and its parameters in an spherical coordinate system [27]. δ_{ij} is the Kronecker delta symbol. For circularly polarized focused Gaussian beams, the BSC's can be easily evaluated by considering symmetry relations [28].

#133019 - $15.00 USD Received 6 Aug 2010; revised 13 Oct 2010; accepted 17 Oct 2010; published 4 Nov 2010

Let us turn our attention to Eqs. (1) and (2) and present, for the first time, the extension of the Mie scattering coefficients for a NRI particle. It is well known that resonance effects can be observed when their denominators approaches zero [23]. This can be mathematically represented by two transcendental equations: $\psi_n'(n_{rel}x)/\psi_n(n_{rel}x) = \mu_p\xi_n'(x)/(\mu n_{rel}\xi_n(x))$ and $\psi_n'(n_{rel}x)/\psi_n(n_{rel}x) = \mu n_{rel}\xi_n'(x)/(\mu_p\xi_n(x))$ for a_n and b_n, respectively. Because n_{rel}/μ_p is always positive, regardless of n_{rel} being positive or negative, the right side of both equations remains unaffected whether we replace n_{rel} by $-n_{rel}$. On the other hand, the left side will be affected by this change in sign, and its slope will be reshaped, i.e., the size parameter associated to the peaks of a_n and b_n will be different for a NRI and a PRI particle with the same (in modulus) refractive index. Note that this change of sign also affects both numerators in Eqs. (1) and (2), so that, in general, a_n and b_n will differ significantly from the PRI case.

As an example, suppose a lossless and simple dielectric spherical PRI particle with n_{rel} = 1.33. Figure 5 shows $Re(a_n)$ and $Im(a_n)$ for n = 1, 4, 9 and 16 and 15 < x < 35, while Fig. 6 is the equivalent of Fig. 5 for n_{rel} = −1.33. We can conclude that, for a specific size parameter, i.e., given a PRI particle of fixed radius, the Mie scattering coefficients a_n will radically differ from the NRI analogue, the same being valid for the coefficients b_n.

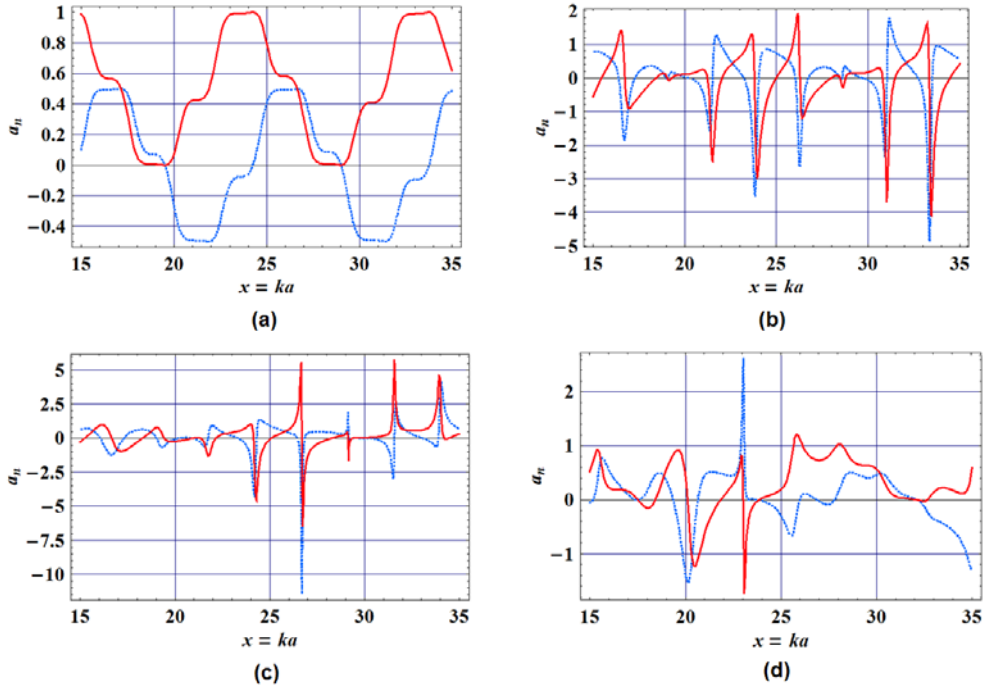

Fig. 5. Real (solid, red) and imaginary (dashed, blue) parts of the Mie scattering coefficient a_n as a function of the size parameter x for n_{rel} = 1.33 and (a) n = 1, (b) n = 4, (c) n = 9 and (d) n = 16. In the framework of the GLMT, the coefficients a_n and b_n modulates the phase and amplitude of the scattered fields.

Thus, the scattered fields will have completely distinct spatial intensity distributions, as it was already pointed out by ray optics in section 2, where the fundamental difference between n_{rel} > 0 and n_{rel} < 0 lied solely in the inversion of Snell's law. Here, the difference in the values of the Mie scattering coefficients accounts for an entire reshape (spatial intensity distribution) of the scattered fields due to its phase and amplitude contributions to each propagating mode.

#133019 - $15.00 USD Received 6 Aug 2010; revised 13 Oct 2010; accepted 17 Oct 2010; published 4 Nov 2010

As already pointed out, we can safely use Eqs. (1) and (2) for the scattering problem of a NRI spherical particle just in the same manner that it has being used so far for the conventional PRI case. Care should be exercised, however, by adequately replacing the permeability of the particle by its negative value whenever $n_{rel} < 0$ or, equivalently, $n_p < 0$. This ensures that the results will effectively represent the correct scattered electromagnetic fields for a NRI particle. The other two possibilities, *viz*., (i) when $n_m < 0$ and $n_p > 0$ or (ii) $n_m < 0$ and $n_p < 0$ could also be analyzed, but we must consider that achieving a liquid medium for which $n_{rel} < 0$ is even more challenging than achieving negative refractive index for a solid particle.

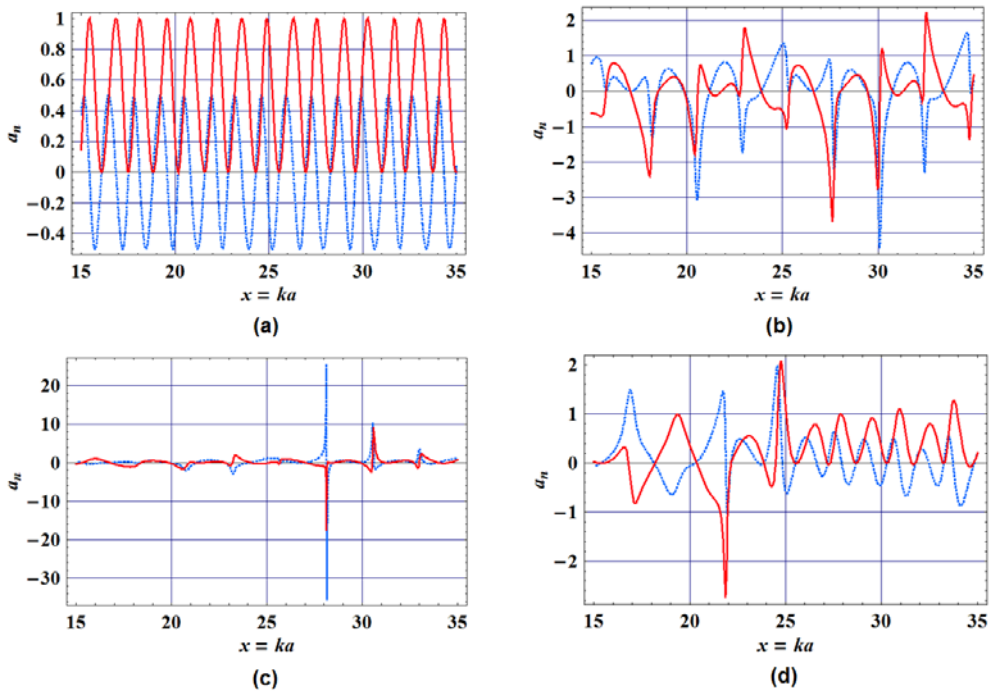

Fig. 6. Real (solid, red) and imaginary (dashed, blue) parts of the Mie coefficient a_n as a function of x for a NRI particle with $n_{rel} = -1.33$ and (a) $n = 1$, (b) $n = 4$, (c) $n = 9$ and (d) $n = 16$. Different phase and amplitudes are observed in comparison with Fig. 5, so that the scattered fields will also be different.

Regardless of the feasibility of such negative refractive index liquid medium, it can be shown from Eqs. (1) and (2) that imposing $n_m < 0$ and $n_p > 0$ or $n_m > 0$ and $n_p < 0$ (or even replacing conditions $n_m > 0$ and $n_p > 0$ by $n_m < 0$ and $n_p < 0$) leads to the same Mie scattering coefficients and, therefore, to the same force profiles. Accordingly, in the ray optics approach, these conditions imply in the same multiple reflection/refraction diagrams observed in previous works [15,16].

4. Radiation pressure calculations for NRI particles

In section 2, it was shown that the inversion of Snell's law leads to different axial force profiles due to the linear momentum transfer from the incident beam to the particle. In this section, we numerically calculate the radiation pressure cross-sections in rectangular coordinates $C_{pr,z}$, $C_{pr,x}$ and $C_{pr,y}$ for right-hand circularly polarized focused Gaussian beams, one of the most common laser beams used in optical trapping experiments and also one of the first to provide full tridimensional trapping of biological particles. A + z-propagation is assumed. The radiation pressure cross-section $C_{pr,z}$ is, then, the longitudinal cross-section

#133019 - $15.00 USD Received 6 Aug 2010; revised 13 Oct 2010; accepted 17 Oct 2010; published 4 Nov 2010

component along the optical axis of the beam, while $C_{pr,x}$ and $C_{pr,y}$ are the transverse components, all of which being intrinsically related to the optical force exerted by the laser beam on the particle.

Radiation pressure formulas for arbitrary laser beams incident on spherical particles are readily available from literature and are usually expressed as [29,30]:

$$C_{pr,z}=\frac{\lambda^2}{\pi}\sum_{n=1}^{\infty}\sum_{p=-n}^{n}\left(\begin{array}{l}\dfrac{1}{(n+1)^2}\dfrac{(n+1+|p|)!}{(n-|p|)!}\mathrm{Re}\left[\begin{array}{l}\left(a_n+a_{n+1}^{*}-2a_n a_{n+1}^{*}\right)g_{n,TM}^{p}\,g_{n+1,TM}^{p*}+\\ \left(b_n+b_{n+1}^{*}-2b_n b_{n+1}^{*}\right)g_{n,TE}^{p}\,g_{n+1,TE}^{p*}\end{array}\right]+\\ p\dfrac{2n+1}{n^2(n+1)^2}\dfrac{(n+|p|)!}{(n-|p|)!}\mathrm{Re}\left[i\left(2a_n b_n^{*}-a_n-b_n^{*}\right)g_{n,TM}^{p}\,g_{n,TE}^{p*}\right]\end{array}\right), \tag{7}$$

$$C=\frac{\lambda^2}{2\pi}\sum_{p=1}^{\infty}\sum_{n=p}^{\infty}\sum_{m=p-1\neq 0}^{\infty}\left(\frac{(n+|p|)!}{(n-|p|)!}\left[\begin{array}{l}\left(S_{m,n}^{p-1}+S_{n,m}^{-p}-2U_{m,n}^{p-1}-2U_{n,m}^{-p}\right)\left(\dfrac{1}{m^2}\delta_{m,n+1}-\dfrac{1}{n^2}\delta_{n,m+1}\right)\\ +\dfrac{2n+1}{n^2(n+1)^2}\delta_{n,m}\left(T_{m,n}^{p-1}-T_{n,m}^{-p}-2V_{m,n}^{p-1}+2V_{n,m}^{-p}\right)\end{array}\right]\right), \tag{8}$$

where

$$\begin{pmatrix}C_{pr,x}\\ C_{pr,y}\end{pmatrix}=\begin{pmatrix}\mathrm{Re}(C)\\ \mathrm{Im}(C)\end{pmatrix} \tag{9}$$

and the coefficients $U_{n,m}^{p},V_{n,m}^{p},S_{n,m}^{p},T_{n,m}^{p}$ read as

$$U_{n,m}^{p}=a_n a_m^{*}g_{n,TM}^{p}\,g_{m,TM}^{p+1*}+b_n b_m^{*}g_{n,TE}^{p}\,g_{m,TE}^{p+1*}, \tag{10}$$

$$V_{n,m}^{p}=ib_n a_m^{*}g_{n,TE}^{p}\,g_{m,TM}^{p+1*}-ia_n b_m^{*}g_{n,TM}^{p}\,g_{m,TE}^{p+1*}, \tag{11}$$

$$S_{n,m}^{p}=\left(a_n+a_m^{*}\right)g_{n,TM}^{p}\,g_{m,TM}^{p+1*}+\left(b_n+b_m^{*}\right)g_{n,TE}^{p}\,g_{m,TE}^{p+1*}, \tag{12}$$

$$T_{n,m}^{p}=i\left(b_n+a_m^{*}\right)g_{n,TE}^{p}\,g_{m,TM}^{p+1*}-i\left(a_n+b_m^{*}\right)g_{n,TM}^{p}\,g_{m,TE}^{p+1*}. \tag{13}$$

A Fortran code was developed for calculating Eqs. (7)–(13) by using the Mie coefficients from Eqs. (1) and (2) and the associated BSC's from Eqs. (5) and (6). This code is available under request. We used Eqs. (1) and (2) to generate the right-hand circularly polarized BSC's, in accordance with [28], but we have not used any symmetry relation. This is more time consuming, but leads to a more ease-to-read program for those not familiar with the GLMT.

4.1. Longitudinal radiation pressure cross-section $C_{pr,z}$

During the first experiments on optical trapping, Ashkin noticed that negative values of $C_{pr,z}$ were possible, depending on the longitudinal distance between the beam waist centre and the centre of the sphere. This was due the gradient of the intensity of the beam [16]. In fact, full tridimensional traps demand $C_{pr,z} = 0$ at some specific point where $C_{pr,x}$ and $C_{pr,y}$ are also zero, thus providing stable equilibrium. For $C_{pr,z}$ always non-negative, a point where $C_{pr,z}$ would eventually be zero corresponds to a point of unstable equilibrium. It is still possible, however, to trap a particle even for $C_{pr,z} \geq 0$, but this would require, for example, alternative schemes, such as levitation traps [31–35]. Here, we shall not be concerned in obtaining an efficient

#133019 - $15.00 USD Received 6 Aug 2010; revised 13 Oct 2010; accepted 17 Oct 2010; published 4 Nov 2010

tridimensional trap for NRI particles, but to examine some differences in their properties relative to PRI particles.

Let us consider that the beam waist centre of a right-hand circularly polarized Gaussian beam is located somewhere along the line $(0,0,z_0)$. The beam has $\lambda = 0.5$ μm, beam waist $w_0 = 5$ μm and illuminates a particle of $n_{rel} = 1.5$. Figure 7(a) shows $C_{pr,z}$ as a function of z_0 for several diameters of the particle, *viz.*, $d = 5$, 10, 20 and 40 μm. The profiles observed are just those expected and already studied by other authors [29].

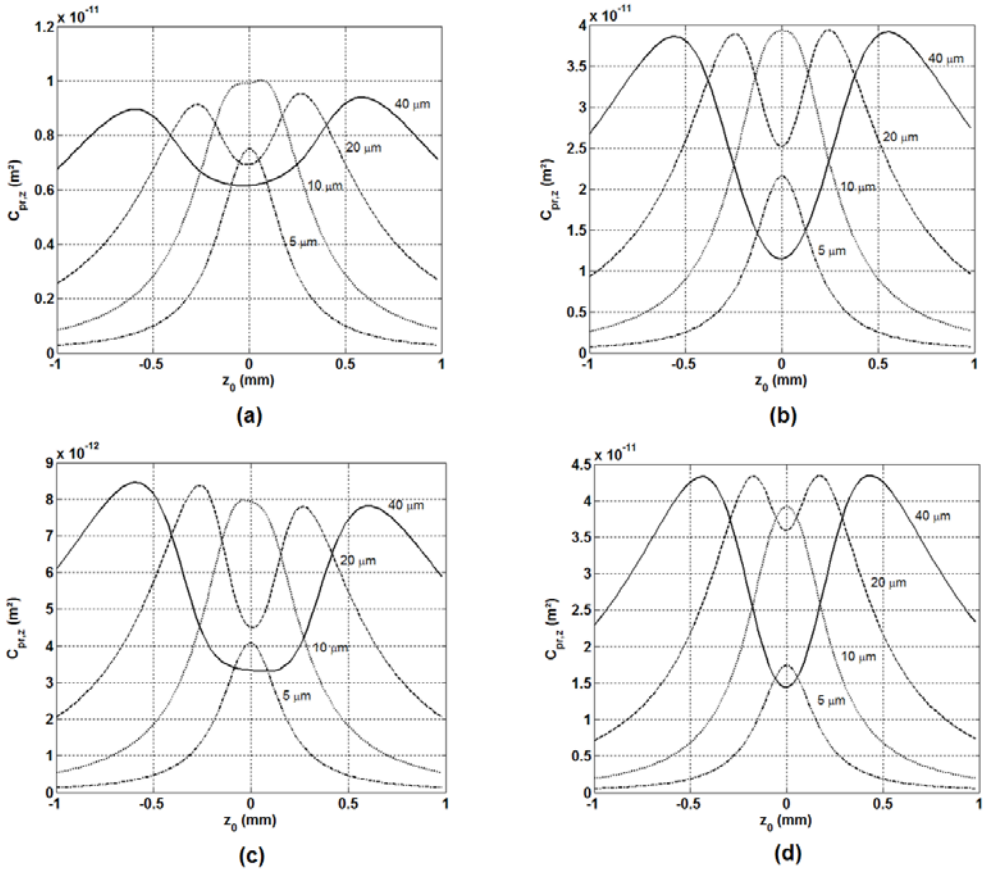

Fig. 7. Longitudinal radiation pressure cross-section $C_{pr,z}$ as a function of z_0 for $x_0 = y_0 = 0$ for (a) $n_{rel} = 1.5$ and (c) $n_{rel} = 1/1.33$. (b) and (d) are the NRI analogues of (a) and (c), respectively.

Now, suppose a NRI particle with $n_{rel} = -1.5$. Figure 7(b) presents the new $C_{pr,z}$ profiles. Although the locations of maxima of $C_{pr,z}$ occurs at about the same position z_0, we can see the disparate values in magnitude for a specific d when compared to the PRI case in Fig. 7(a). For example, for $d = 40$ μm, maxima of $C_{pr,z(\mathrm{NRI})}$ can be seen at $z_0 \approx 5.64 \times 10^{-4}$ m and -5.45×10^{-4} m, whereas maxima of $C_{pr,z(\mathrm{PRI})}$ occur at $z_0 \approx 6.04 \times 10^{-4}$ m and -5.84×10^{-4} m. The ratio of these maxima are $C_{pr,z(\mathrm{NRI})}|_{z0 \approx 5.64 \times 10\text{-}4\ \mathrm{m}} / C_{pr,z(\mathrm{PRI})}|_{z0 \approx 6.04 \times 10\text{-}4\ \mathrm{m}} \approx 4.31$ and $C_{pr,z(\mathrm{NRI})}|_{z0 \approx -5.45 \times 10\text{-}4\ \mathrm{m}} / C_{pr,z(\mathrm{PRI})}|_{z0 \approx -5.84 \times 10\text{-}4\ \mathrm{m}} \approx 4.17$, representing a much stronger longitudinal radiation pressure for the NRI particle. It must be emphasized that the longitudinal radiation pressure cross-section can be significantly different for the NRI case when compared with the conventional PRI analogue. Again, this is due to the numerical differences in the Mie coefficients observed in the previous section or, equivalently, due to the distinct reflection/transmission diagram for an incident ray in ray optics.

#133019 - $15.00 USD Received 6 Aug 2010; revised 13 Oct 2010; accepted 17 Oct 2010; published 4 Nov 2010

As a second example, Fig. 8(a) is a reproduction of Fig. 8.11 from [36] using the same parameters of the original work, i.e., a right-hand circularly polarized focused Gaussian beam with $\lambda = 0.3682$ μm, $w_0 = 1.8$ μm and $a = 3.75$ μm. Six values of n_{rel} are used. The analogous NRI case with the same relative refractive indices (in modulus) is shown in Fig. 9(b) for comparison. The following comments can be made regarding both figures: first, one notices negative longitudinal radiation pressure cross-section $C_{pr,z}$ for positive n_{rel} [Fig. 8(a)], whereas $C_{pr,z} > 0$ for all $n_{rel} < 0$ [Fig. 8(b)]; second, the difference in magnitude (order of 10^2) of $C_{pr,z}$ for the NRI and the PRI cases and the similitude of the slopes (superposed curves) for small variations of n_{rel} when $n_{rel} < 0$. Physical interpretations regarding the shape of the slopes of $C_{pr,z}$ in Figs. 7 and 8 for $n_{rel} < 0$, however, remains the same for $n_{rel} > 0$ and can be found elsewhere [29].

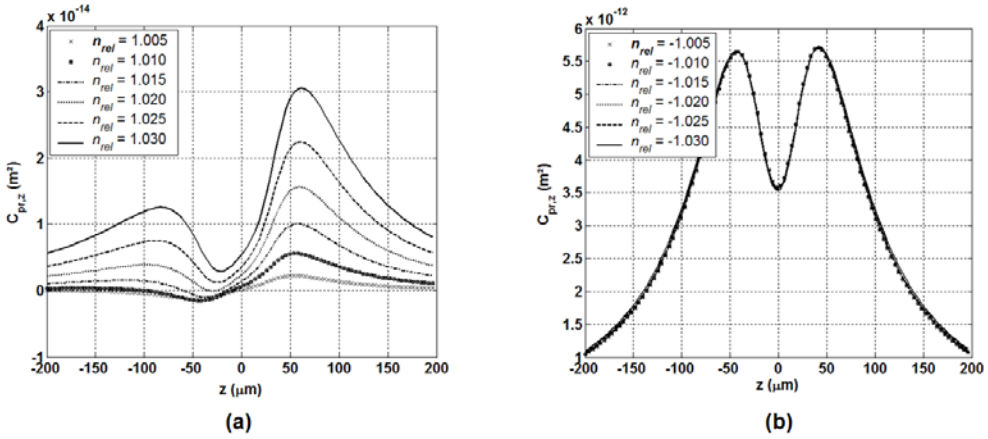

Fig. 8. (a) $C_{pr,z}$ for several values of n_{rel} assuming a PRI particle with radius $a = 3.75$ μm immersed on a focused Gaussian beam with $\lambda = 0.3682$ μm and $w_0 = 1.8$ μm. The same relative refractive indices were used in (b) for a NRI particle with the same radius as (a). The beam is shifted along its optical axis, i.e., $x_0 = y_0 = 0$.

It must be emphasized that negative longitudinal radiation pressure cross-section can also be achieved with lossless NRI spherical particles, including the case $n_{rel} = -1$, which has been under intense investigation due to its incredible, new and until recently unimaginable possibility of applications, such as the famous perfect lens idealized by Pendry [37]. So, consider as a final example a focused Gaussian beam with $\lambda = 1064$ nm (a typical injurious laser beam used in biological experiments) and spot $w_0 = 1000$ nm. These values coincide, at least for an on-axis beam, with the approximate theoretical limit of applicability of the localized beam model to GLMT calculations, as the parameter $s = 1/kw_0 = 0.169$ [26,27]. Calculations of $C_{pr,z}$ for $n_{rel} = -1$ for size parameters $s_p = 50$, 100, 150 and 200 (*viz.*, diameters of $d \approx 8.47$, 16.93, 25.40 and 33.87 μm, respectively) are shown in Fig. 10, and we can clearly see negative values of $C_{pr,z}$ and three points of stable equilibrium (indicated by arrows) concerning only the longitudinal pushing of the particle.

4.2. Transverse radiation pressure cross-sections $C_{pr,x}$ and $C_{pr,y}$

In common optical trapping systems, auxiliary and biological particles always have positive refractive index, being an easy task to predict their direction of displacement due to the previous knowledge of the gradient intensity of the incident beam. Then, if the relative refractive index between the particle and its surrounding medium $n_{rel} > 1$, an optical trap is to be expected with the particle localized at points of stable equilibrium or, as an another perspective, at high intensity regions of the laser beam. On contrary, if $n_{rel} < 1$, then it will invariably be directed away from these high intensity regions. In the case of focused Gaussian beams, this last situation can be interpreted as a limitation in achieving an efficient trap. There

#133019 - $15.00 USD Received 6 Aug 2010; revised 13 Oct 2010; accepted 17 Oct 2010; published 4 Nov 2010

are, of course, other types of beams (*viz*., Bessel beams) where a set of spatial positions (low intensity regions of the beam) exists in which a particle possessing $n_{rel} < 1$ can still be trapped, again allowing three- or two-dimensional manipulation of particles.

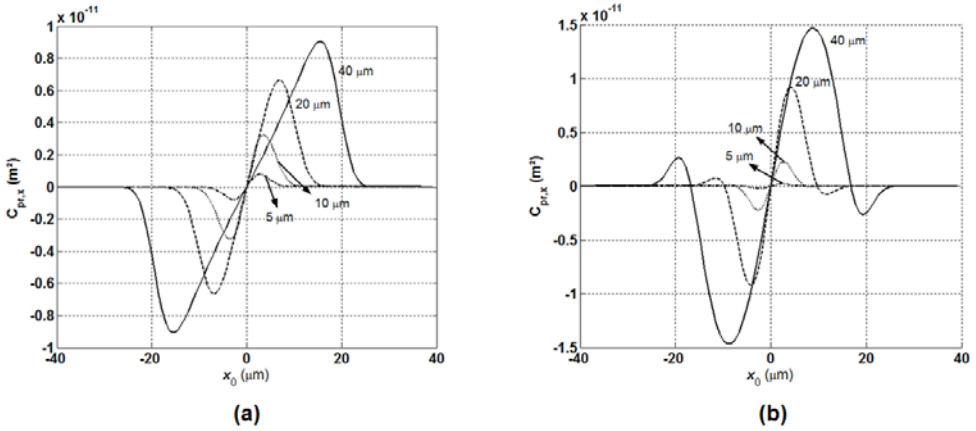

Fig. 9. (a) $C_{pr,x}$ for several diameters of a PRI particle with $n_{rel} = 1.5$. The beam is shifted along x with $y_0 = z_0 = 0$, x_0 being the transverse distance between the optical axis and the centre of the particle. (b) The NRI analogue with $n_{rel} = -1.5$.

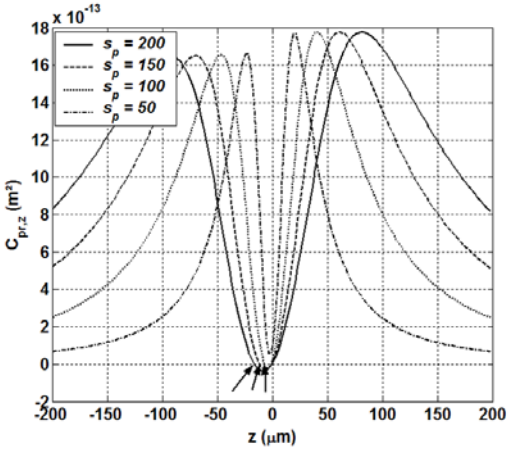

Fig. 10. (a) $C_{pr,z}$ for a NRI particle with $n_{rel} = -1$ and four different size parameters. The incident beam is a focused Gaussian beam with $\lambda = 1064$ nm and $w_0 = 1.0$ μm. The beam is shifted along its optical axis, i.e., $x_0 = y_0 = 0$.

While the direction of displacement of a positive refractive index particle is relatively simple to determine, the situation for a negative refractive index particle is a little bit more involved. Suppose, for example, a NRI particle with a given refractive index n_p. We can conclude, by recalling the previous analysis of section 2, that the relative distance between the focal point and the centre of the particle is a determinant variable in calculating axial forces. While these forces seem to be attractive for short relative distances, as the particle goes away from the focus, they may become repulsive, a behavior which would never be expected for a PRI particle but that can be easily predicted for a NRI particle using simple ray optics considerations. Thus, we cannot try to use only gradient intensity considerations (together with the well-known repulsive/attractive critical limits $n_{rel} < 1$ and $n_{rel} > 1$) when studying NRI particles immersed in a positive refractive index medium.

#133019 - $15.00 USD Received 6 Aug 2010; revised 13 Oct 2010; accepted 17 Oct 2010; published 4 Nov 2010

In the framework of the GLMT, axial forces are intrinsically related to the transverse radiation pressure cross-sections $C_{pr,x}$ and $C_{pr,y}$, so that we can use Eqs. (5) and (6), adapted for a right-hand circularly polarized focused Gaussian beam [28], in the set of Eqs. (8)–(13) for calculating $C_{pr,x}$ and $C_{pr,y}$ for a focused Gaussian beam, just as we did for the longitudinal radiation pressure cross-section $C_{pr,z}$ in the last subsection. Let us again assume a right-hand circularly polarized Gaussian beam, with $\lambda = 0.5$ μm and $w_0 = 5$ μm, illuminating a particle of $n_{rel} = 1.5$. Figure 9(a) shows how $C_{pr,x}$ changes as we shift the beam along x for four possible diameters $d = 40$, 20, 10 or 5 μm of a PRI particle with $n_{rel} = 1.5$. Because now it is the beam which is spatially displaced (in section 2, by varying γ we were shifting the particle in space), here $C_{pr,x} > 0$ ($C_{pr,x} < 0$) implies in attractive (repulsive) forces for x_0 or $y_0 > 0$. As we can clearly see, PRI particles will always be pushed towards the high intensity region of the beam, regardless of its diameter. But if we replace them by NRI particles with $n_{rel} = -1.5$, as in Fig. 9(b), besides the raise in amplitude, a new axial force profile appears. As we had already pointed out, depending upon the diameter of the NRI particle and its relative distance to the optical axis (beam waist centre), both attractive and repulsive axial forces are exerted on the particle. For example, when $d = 40$ μm and $x_0 < -16.6$ μm, the particle will suffer an influence of a repulsive force whose maximum, however, is only 18.3% that of the attractive force observed for -16.6 μm $< x_0 < 0$. Figure 11 corresponds to Fig. 9, but for particles whose relative refractive index is smaller than |1| ($n_{rel} = \pm 0.5$), and Figs. 12 and 13 are the equivalent of Figs. 9 and 11, respectively, but now for $C_{pr,y}$ and a displacement of the laser beam along y.

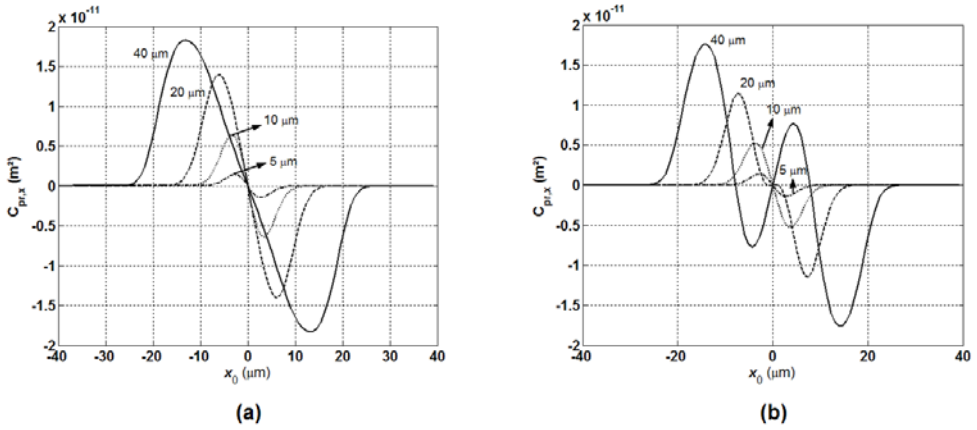

Fig. 11. $C_{pr,x}$ for several diameters of a PRI particle with (a) $n_{rel} = 0.5$ and (b) $n_{rel} = -0.5$. This corresponds to Fig. 9 but now for $|n_{rel}| < 1$.

If we focus our attention into Figs. 9(a), 11(a), 12(a), and 13(a), we will see the expected profile for a PRI particle under the influence of a right-hand circularly polarized focused Gaussian beam: whenever $n_{rel} > 1$, the gradient of intensity of the beam generates attractive forces and, for $0 < n_{rel} < 1$, these forces are repulsive. But there is something more to which we should look at carefully, regarding the optical regime and the vector nature of the incident beam. First, the amplitudes observed in Figs. 9(a) and 12(a) and also in Figs. 11(a) and 13(a) are close to each other, so that we should ask ourselves if this is correct. Looking back at the literature, Gouesbet *et al* [29] found different amplitudes for these same parameters. But a moment thought would lead us to conclude that this should not happen because of the symmetry of the incident beam, its polarization (circular) and the electromagnetic properties and the ratio d/λ of all particles (e.g., for $d = 5$ μm, $d/\lambda = 10$, which would ultimately define the lower limit of applicability of geometrical optics). Obviously, if a linearly polarized beam is used, then $C_{pr,x}$ and $C_{pr,y}$ differ in magnitude, depending upon the relative direction of displacement between the beam waist centre and the centre of the particle. These

#133019 - $15.00 USD Received 6 Aug 2010; revised 13 Oct 2010; accepted 17 Oct 2010; published 4 Nov 2010

considerations are immediately extended to the NRI case, *viz.*, Figs. 9(b), 11(b), 12(b), and 13(b).

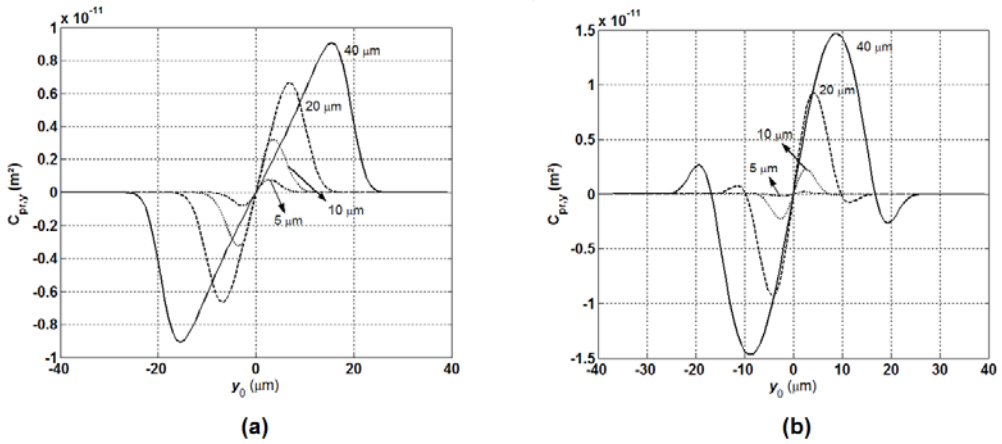

Fig. 12. (a) $C_{pr,y}$ for several diameters of a PRI particle with n_{rel} = 1.5. The beam is shifted along y with $x_0 = z_0 = 0$, y_0 being the transverse distance between the optical axis (beam waist centre) and the centre of the particle. (b) The NRI analogue with n_{rel} = –1.5.

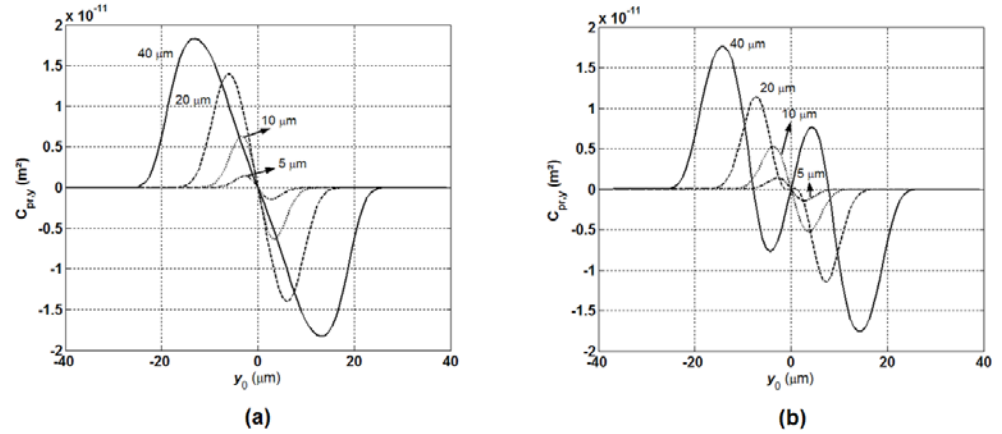

Fig. 13. $C_{pr,y}$ for several diameters of a PRI particle with (a) n_{rel} = 0.5 and (b) n_{rel} = –0.5. This corresponds to Fig. 12 but now for $|n_{rel}| < 1$.

Because linear momentum is transferred to a NRI particle in a slightly different way, the Mie scattering coefficients alter the values of the longitudinal and transverse radiation pressure cross-sections in Eqs. (7) and (9), respectively, thus leading to new force profiles. Thus, the GLMT reflects the new scattered field for a NRI particle.

When the relative refractive index is –1.5, one can see from Figs. 9(b) and 12(b) that both repulsive and attractive transverse forces can act on the particle, depending on the relative distance x_0 between the beam waist centre and the centre of the particle. Because d/λ is always higher than or equal to 10, a qualitative explanation can be done, based on geometrical optics considerations. First, consider d = 40 μm. This implies $d/w_0 = 8$, so that, for short relative distances x_0, the rays impinge the particle with small incidence angles, thus giving rise to attractive forces. This can be better appreciated by considering individual transverse forces analogous to Fig. 2 but for n_{rel} = –1.5, graphically represented by a dotted curve in Fig. 14. As the beam waist centre gets close to x_0 = 17 μm, i.e., close to the radius of the particle, repulsive individual transverse forces prevails, as expected from Fig. 14 for high incidence

#133019 - $15.00 USD Received 6 Aug 2010; revised 13 Oct 2010; accepted 17 Oct 2010; published 4 Nov 2010

angles. Notice, however, that the peak of this repulsive force ($C_{pr,x}$ ≈2.70 × 10^{-12} m^2 at x_0 ≈19.41 μm) is relatively low compared to the peak observed in the region of attractive force ($C_{pr,x}$ ≈14.69 × 10^{-11} m^2 at x_0 ≈9.11 μm). As d/w_0 decreases, so does the amplitude of the transverse force. When $d/w_0 = 1$ (e.g., $d = 5$ μm), repulsive forces will take place for $x_0 > 7.52$ μm but, due to their low amplitude, this is not readily seen in Fig. 9(b). For Figs. 11(b) and 13(b), we must further consider the fact that, above $\theta_i > 0.5236$ rad, an incident ray will suffer total reflection and, according to the solid curve in Fig. 14, higher repulsive forces can be expected. This is, in fact, true, as shown for $C_{pr,x}$ and $C_{pr,y}$ in Figs. 11(b) and 13(b), respectively. Finally, because of total reflection, it is not always possible to trap NRI particles with $-1 < n_{rel} < 0$. For the parameters used, NRI particles with $n_{rel} = -0.5$ and $d = 5$ or 10 μm would always be directed away from the beam waist centre. Thus, as $|n_{rel}|$ decreases, repulsive forces prevail. This is illustrated in Fig. 15 for six different values of n_{rel}.

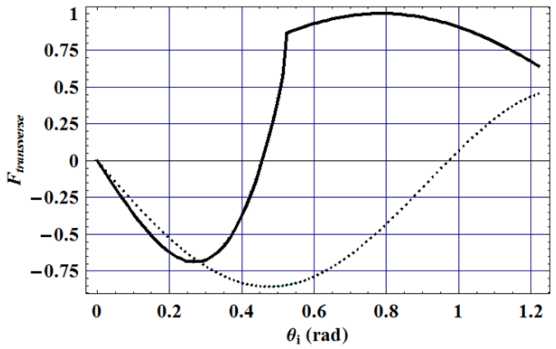

Fig. 14. Normalized (over $n_m P/c$) individual transverse force $F_{transverse}$ as a function of θ_i for both $n_{rel} = -1.5$ (dotted) and -0.5 (solid). For the last case, total reflection occurs for $\theta_i > 0.5236$ rad.

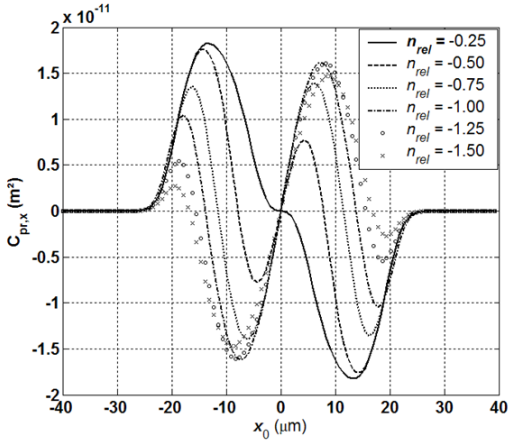

Fig. 15. $C_{pr,x}$ as a function of the displacement x_0 and the relative refractive index n_{rel} for a NRI particle with $d = 40$ μm.

5. Conclusions

Forces and radiation pressure cross-sections were systematically analyzed for lossless negative refractive index spherical and simple particles. It was shown, for the first time in the literature, both by ray optics and by adopting the generalized Lorenz-Mie theory with the integral localized approximation, that the forces and radiation pressure cross-sections behave

#133019 - $15.00 USD Received 6 Aug 2010; revised 13 Oct 2010; accepted 17 Oct 2010; published 4 Nov 2010

quite differently due to the new linear momentum transfer characteristic that takes place for NRI particles.

In the ray optics, the inversion of Snell's law accounts for individual forces whose dependence with the incidence angle reveals new capabilities in trapping NRI particles, because both attractive and repulsive forces can happen depending upon how the ray impinges the particle. This characteristic is just unrealizable for PRI particles, as the transmission angle is always "positive". In the framework of the generalized Lorenz-Mie theory, a NRI particle will present different force profiles when compared to the conventional PRI optical trapping because of the new scattered field, theoretically represented by the Mie scattering coefficients.

Negative longitudinal radiation pressure cross-sections can also be obtained in the NRI case by suitably choosing the relative refractive index of the particle and its dimensions relative to the parameters of the incident laser beam. It is not possible, however, to formulate an explanation of NRI optical trapping based solely on the relative refractive index of the particle and the gradient intensity of the beam in the optical regimes of this paper.

The fact that repulsive transverse forces prevail over attractive ones as the relative distance between the beam waist centre and the centre of the NRI particle may turn NRI optical trapping into an experimentally more difficult task, because care would have to be exercised in spatially manipulating the laser beam so that an effective optical trap is produced.

All results presented here were obtained for a (right hand) circularly polarized focused Gaussian beam. Other types of polarization could be implemented, as well as other laser beams such as Bessel and Laguerre-Gaussian beams. In fact, the whole theory of optical trapping, including resonance effects and torque properties, must be revised for NRI optical trapping. These studies are currently under investigation.

The question of how to experimentally achieve a homogeneous, linear, isotropic, lossless spherical negative refractive index material is still open. Resonant tridimensional metamaterial structures possessing negative refractive index have been theoretically demonstrated, but the difficulty of realizing theoretical and experimental non-resonant tridimensional NRI materials may be overcome in the forthcoming years.

Acknowledgments

The authors wish to thank Fundação de Amparo à Pesquisa do Estado de São Paulo (FAPESP) under contracts 2009/54494-9 (L. A. Ambrosio's post doctorate grant) and 2005/51689-2 (CePOF, Optics and Photonics Research Center), for supporting this work.

#133019 - $15.00 USD Received 6 Aug 2010; revised 13 Oct 2010; accepted 17 Oct 2010; published 4 Nov 2010